# Optical excitation and detection of picosecond acoustic pulses in liquid mercury

O. B. Wright
*Department of Applied Physics, Graduate School of Engineering, Hokkaido University, Sapporo 060-8628, Japan*

B. Perrin
*Institut des NanoSciences de Paris, Université Paris 6, UMR 7588 CNRS, 140 Rue de Lourmel, 75015 Paris, France*

O. Matsuda
*Department of Applied Physics, Graduate School of Engineering, Hokkaido University, Sapporo 060-8628, Japan*

V. E. Gusev
*Laboratoire de Physique de l'Etat Condensé, Faculté des Sciences, Université du Maine, UMR-CNRS 6087, Av. O. Messiaen, 72085 Le Mans, France*

(Received 7 February 2008; revised manuscript received 18 June 2008; published 25 July 2008)

Ultrashort optical pulses are used to excite and interferometrically detect picosecond longitudinal-acoustic pulses in thin films of liquid mercury sandwiched between sapphire plates. We show that the shape of the strain pulses in the mercury can be directly measured through ultrafast changes in optical reflectivity. By analyzing consecutive acoustic echoes, we derive the dispersion of the ultrasonic attenuation and sound velocity for this liquid at frequencies up to 10 GHz. Significant effects of structural relaxation are observed and are compared to a simple model that indicates the presence of picosecond relaxation times in mercury.

DOI: 10.1103/PhysRevB.78.024303 PACS number(s): 62.80.+f, 61.25.Mv, 43.35.+d, 66.10.cd

## I. INTRODUCTION

Ultrasonic propagation in liquids is of much interest because the dispersion of the sound velocity and acoustic attenuation is closely related to the rate at which the liquid can recover from a local change in strain, this rate being dependent on the microscopic ordering in the liquid. At high enough frequencies the local atomic environment remains frozen on the passage of an acoustic strain wave, leading to a different—generally higher—elastic modulus at the limit of high frequency compared to at lower frequencies. This phenomenon, known as structural relaxation, can therefore be studied by frequency-dependent ultrasonic velocity and attenuation measurements.[1,2] Conventional ultrasonics techniques with piezoelectric excitation and detection,[3,4] as well as nanosecond laser acoustics,[5,6] can be used effectively up to ~1 GHz for the study of longitudinal-acoustic waves in liquids, both transparent and opaque. Frequencies up to ~20 GHz in transparent liquids are accessible by Brillouin scattering, a technique relying on the spontaneous or stimulated scattering of light by phonons.[7–10] In addition, inelastic x-ray[11–13] or neutron-scattering measurements[13,14] can be implemented to probe vibrational dynamics in the ~300 GHz to terahertz regime in liquids.

A new addition to this array of techniques for probing structural relaxation in liquids is the method of picosecond laser acoustics, initially developed for solids.[15–20] Like impulsive stimulated light scattering,[21] it is a time domain technique and has the potential for measurements on liquids up to the terahertz range. The principle relies on generating picosecond ultrasonic pulses using ultrashort pump light pulses and then detecting the ultrasonic pulses using synchronous probe light pulses. It was recently proved to be useful for observing the propagation of longitudinal-acoustic waves in water at ~4 GHz by monitoring backscattered probe light from the sound in the liquid.[22] Reflections from solid-liquid interfaces at frequencies up to 300 GHz have also been studied by this technique with acoustic incidence from the solid.[23] Laser acoustics at megahertz frequencies has also been successful for investigating absorbing liquids, although these frequencies are in general too low to be useful for studies of structural relaxation in many liquids.[24] Sound generation with ultrashort light pulses has also been investigated in the ablative regime in transparent liquids.[25]

To investigate structural relaxation in opaque liquids, particularly in liquid metals, one would ideally like to measure the sound velocity and the ultrasonic attenuation over a wide frequency range. This has proven difficult in the gigahertz range owing to the short optical penetration depths that broaden the optical spectra in Brillouin scattering.[13,26] However, this frequency range is of particular interest in monatomic liquids and those of relatively low molecular weight because it corresponds to the regime of the onset of structural relaxation. In this paper we describe a pulse-echo implementation of picosecond laser acoustics to probe the ultrasonic dispersion in liquid Hg up to 10 GHz. The sound pulses are directly generated in a thin film of liquid Hg sandwiched between two sapphire plates, allowing us at the same time to probe the generation of sound in a liquid metal with ultrashort light pulses. The case of liquid Hg is particularly interesting because it is known to exhibit a huge positive dispersion effect: the longitudinal sound velocity increases by ~50% at terahertz frequencies.[13] However, the way the sound velocity rises from its low-frequency value (<1 GHz) to its high-frequency value is completely unknown.

In addition to investigating the structural relaxation, we also describe a method for direct measurement of the shape of the strain pulses propagating in the mercury. This method exploits the short optical penetration depth compared to the

 

spatial extent of the acoustic pulses in mercury and allows the strain pulse shape to be measured from photoelastically induced changes in optical reflectivity at a buried interface. This is simpler than previous methods for strain pulse shape measurement in picosecond laser acoustics that rely on the optical phase variation.[17,27] We also make use of a theoretical model that accounts for the interface displacements in the sample and the photoelastic effect in the mercury to relate these reflectivity changes to measured optical phase changes.

In Sec. II we describe the experimental technique. In Sec. III we describe the experimental results for the acoustic echoes and describe how to use them to interpret the shape of the generated longitudinal strain pulses in the liquid Hg. In Sec. IV we present detailed results for both the first and second echoes and derive the acoustic dispersion in liquid Hg by comparison of successive echoes. In Sec. V we discuss the results for the acoustic dispersion and present our conclusions.

## II. EXPERIMENTAL TECHNIQUE

The liquid Hg (Ref. 28) is clamped to a thickness of $\sim 1$ $\mu$m between two flat sapphire plates of thickness 3 mm with (0001) surfaces of rms roughness of $\sim 3$ nm as determined by atomic force microscopy. The choice of sapphire, with longitudinal sound velocity $v_l = 11\,100$ ms$^{-1}$ and density $\rho_0 = 3990$ kg m$^{-3}$,[29] localizes the sound within the acoustically mismatched Hg ($v_l = 1450$ ms$^{-1}$ and $\rho_0 = 13\,500$ kg m$^{-3}$) (Ref. 3) and avoids a significant photoelastic coupling to the strain propagating in the plates (below 10 GHz). In the clamped state the plates are sufficiently parallel (within $\sim 0.01°$) to prevent the perturbation of acoustic echo shapes. The plates are mounted vertically, but the relatively high surface tension of the Hg prevents it leaking.

Optical pump pulses of duration of 200 fs, wavelength of 750 nm, pulse energy of $\sim 2$ nJ, and with a repetition rate of 82 MHz are focused on the Hg surface to a 35 $\mu$m diameter spot at full width at half maximum. Thermal expansion occurs as the acoustic strain propagates out of the laser-heated region. For our laser spot size ($\gg$ initially heated depth), longitudinal strain pulses in approximately plane wave form travel directly away from the Hg-sapphire interface in both directions. The strain pulse duration in the Hg is determined by the sound propagation time across the initially heated depth, which depends on the optical-absorption depth in Hg [$\zeta = 10.1$ nm at 750 nm[30]] and on electron and thermal diffusion,[15,27,31,32] as discussed later. The transient and steady-state temperature rises of the Hg above our room-temperature conditions are $\sim 40$ and 15 K, respectively.[33] In contrast to previous nanosecond laser acoustics experiments in liquid Hg,[34] the conditions for generation here are nondestructive. Related experiments on other liquid metals have also been carried out in the megahertz regime.[35,36]

Synchronous delayed optical probe pulses of the same wavelength and spot size and with a pulse energy of $\sim 0.15$ nJ measure the transient changes in reflectance and phase to an accuracy of $\sim 10^{-5}$ in a Mach-Zehnder interferometer arrangement incorporating two photodiodes.[37] Optical delays are produced in a delay line and also using a vibrating corner cube, the latter facilitating measurements of single acoustic echoes. Two different optical incidence configurations are adopted: (1) with both the pump and probe beams focused to the same spot at the angles of incidence 0° and $\sim 10°$, respectively, and (2) with the pump and probe beams incident from opposite sides of the sample at the same angles of incidence (see insets of Figs. 1 and 2, respectively). The pump beam is chopped (at 1 MHz), and lock-in detection is used to improve the signal-to-noise ratio.

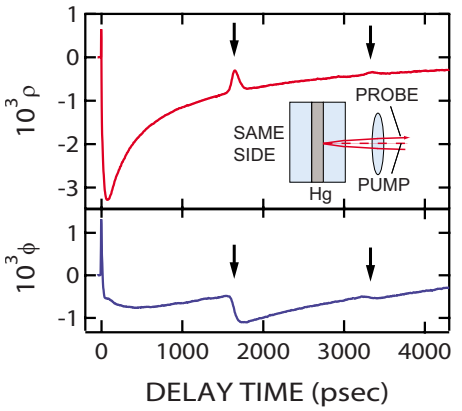


FIG. 1. (Color online) Experimental variations in the optical amplitude-reflection coefficient $\rho$ and the optical phase $\delta\phi$ for a thin film of liquid Hg with a nominal thickness of 1.22 $\mu$m when pumping and probing from the same side. The arrows indicate the positions of the first and second echoes. The inset shows a schematic diagram of the optical incidence on the Hg film with the optical pump and probe beams on the same side of the sample.

For small changes in probe reflectance, the relative change in the complex amplitude-reflection coefficient $r$ of

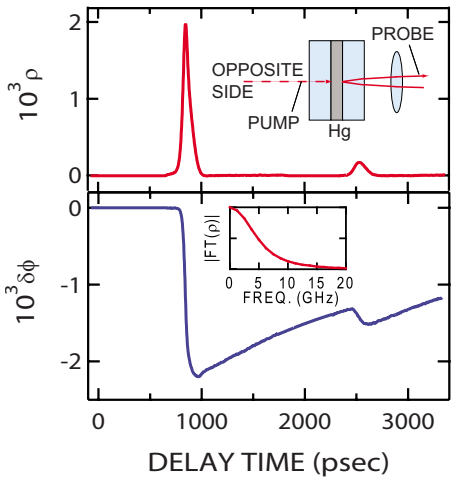


FIG. 2. (Color online) Experimental variations in the optical amplitude-reflection coefficient $\rho$ and the optical phase $\delta\phi$ for a thin film of liquid Hg with a nominal thickness of 1.20 $\mu$m when pumping and probing from opposite sides of the sample. The first and second echoes are evident. Inset: normalized magnitude of the frequency spectrum for $\rho$ for the first echo obtained from the temporal Fourier transform of $\rho(t)$. The inset shows a schematic diagram of the optical incidence on the Hg film with the pump beam on the opposite side to the probe beam.

the sample is given by $\delta r/r=\rho+i\delta\phi$, where $\rho$, the real part, is related to the relative intensity change $\delta R/R$ through the equation $\rho=\delta R/(2R)$ (where $R$ is the reflectivity for intensity), whereas $\delta\phi$, the imaginary part, is the optical phase change. Detection of $\rho$ and $\delta\phi$ gives two independent measures of the picosecond acoustic pulses, allowing the photoelastic response of the sample to be probed more effectively.[19,32,38,39]

## III. RESULTS AND STRAIN PULSE SHAPE MEASUREMENT

Typical results for the variations $\rho(t)$ and $\delta\phi(t)$ are shown in Fig. 1 for a film of Hg with a thickness of 1.22 $\mu$m when pumping and probing from the same side (see inset of Fig. 1). Near delay time $t=0$, a sharp spike arising from the excitation and subpicosecond decay of nonequilibrium electrons in the Hg is evident in both the variations of $\rho$ and $\delta\phi$. This is followed by changes (positive for $\rho$ and negative for $\delta\phi$) that are determined for $\rho$ by the temperature changes in the Hg and sapphire and their decay through thermal diffusion and determined for $\delta\phi$ by temperature changes and by the relaxation of the thermal expansion in the region of the interface. The first and second acoustic echoes are indicated by the arrows in Fig. 1. The 1.22 $\mu$m thickness of the Hg is calculated from the acoustic round trip time using the known value of $v_l$, assumed here to be equal to that measured at lower acoustic frequencies up to ~1 GHz.[3] The acoustic echoes in reflectance $(\rho)$, ~200 ps in duration, have a unipolar shape, whereas the echoes in phase have a rounded steplike shape. The duration of the acoustic echoes is consistent with the presence of frequency components up to ~10 GHz.

In the above arrangement the relevant propagation distance for the first echo is twice the Hg film thickness. In order to investigate smaller distances we use pumping and probing from opposite sides of the sample (see inset of Fig. 2), as illustrated by typical results for a film of Hg with a thickness of 1.20 $\mu$m in Fig. 2. We again refer to the acoustic pulse arrivals as the first and second echoes, although the first echo is not a returning pulse but a transmitted pulse in this case. Since the excitation and detection regions are now separate, there is no spike near $t=0$, and for $\rho$ there is negligible background variation. For $\delta\phi$ there is still a background variation caused by the relaxation of the strain distribution in the near-surface region that is produced by the reflection of the unipolar strain pulses at the Hg-sapphire interface.

To understand the shapes of these echoes, we examine the theory of strain pulse generation, propagation, and detection for a boundary between an opaque material and a transparent solid. Picosecond acoustics experiments with a similar optical detection configuration have previously been carried out on silica-Ge and silica-metal boundaries.[40–42] Since the acoustic impedance ($Z=\rho_0 v_l$, where $\rho_0$ is the mass density) of the sapphire ($Z_2=4.3\times10^7$ kg m$^{-2}$ s$^{-1}$)[29] is larger than that of the Hg ($Z_1=1.96\times10^7$ kg m$^{-2}$ s$^{-1}$),[3] the acoustic strain reflection coefficient from the Hg-sapphire interface (with incidence from the Hg) is positive: $r_{ac}$

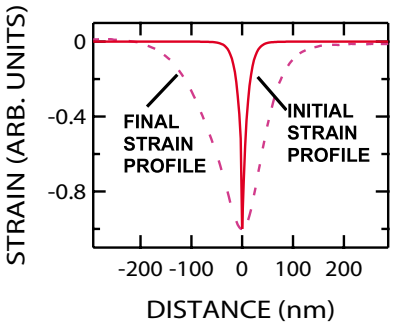


FIG. 3. (Color online) Calculated normalized initial spatial profile of the strain pulse in the sample according to a thermoelastic model ignoring thermal and electron diffusions (solid line). This is compared with the final strain profile for a liquid Hg film with a nominal thickness of 1.48 $\mu$m, as derived from the experimental $\rho(t)$ using pumping and probing from the opposite side of the sample (dashed line). The distance is defined as positive toward the right in the inset of Fig. 2, and the zero of distance is chosen to correspond to the minimum of the strain.

$=(Z_2-Z_1)/(Z_2+Z_1)\approx0.39$. Simple thermoelastic generation theory[15,40] in the absence of diffusion processes leads to a unipolar strain pulse shape (for $r_{ac}>0$) in the form

$$\eta(z,t)=-\frac{1}{2}\eta_0 e^{-|z-v_l t|/\zeta} \text{ for } z>v_l t, \tag{1}$$

$$\eta(z,t)=-\frac{1}{2}\eta_0 r_{ac} e^{-|z-v_l t|/\zeta} \text{ for } z<v_l t, \tag{2}$$

where

$$\eta_0=\frac{B\beta(1-R)Q}{AC\zeta\rho_0 v_l^2}=\frac{\beta(1-R)Q}{AC\zeta}. \tag{3}$$

Here we have introduced the bulk modulus $B$ $(=\rho_0 v_l^2$ in liquids), the volume thermal-expansion coefficient $\beta$, the heat capacity per unit volume $C$, the optical-absorption depth $\zeta$, and the pump spot area $A$.[43] The coordinate $z$ is directed away from the interface (at $z=0$) in the Hg. Equations (1) and (2) apply when the strain pulse has left the near-surface region. The shape of the predicted strain pulse in space is shown by the solid line in Fig. 3. The strain is compressive, and the leading edge of the strain pulse is about 2.6 $(1/r_{ac})$ times stronger than the trailing edge (although the eye is not good at discerning the difference on the scale in Fig. 3). The predicted spatial width of the pulse is of the order of $\zeta(\sim10$ nm), and the temporal width is $\sim\zeta/v_l(\sim7$ ps). The strain amplitude $\eta_0/2\sim7\times10^{-3}$ for the pump fluences used in experiment predicted using literature values for the physical constants.[30,44] This relatively large value compared to that obtained with solid metals at similar optical pump fluences owes much to the relatively high thermal-expansion coefficient of liquid Hg, $\beta=1.8\times10^{-4}$ K$^{-1}$,[44] not atypical for liquids. However, the effect of electron and thermal diffusion will reduce the prediction by a factor $\sim\zeta'/\zeta$, where $\zeta'$ is an effective penetration depth.

To estimate these effects let us consider separately the cases of electron and thermal diffusions. A more rigorous

treatment is possible using the two-temperature model that has been applied to solids, in which the electron and lattice temperatures are considered to be independent but coupled. This model has been implemented to explain picosecond acoustic echo shapes in similar experiments on Au, Ag, Cu, Ni, and Cr.[27,32,45,46] However, we shall content ourselves here with a qualitative discussion because this will suffice to show that the ultrafast dynamics turns out to have a negligible effect on the acoustic echo shapes for the acoustic propagation distances ($\sim 1$ $\mu$m) in the present study. After the optical pump pulse arrival and during a time of the order of the energy relaxation time of the nonequilibrium electrons (given by $\tau_e = C_e/g$, where $C_e$ is the electron specific-heat capacity per unit volume and $g$ is the electron-phonon coupling constant), nonequilibrium electrons diffuse and transport their energy to a typical depth $z_e = (D_e \tau_e)^{1/2} = (\kappa_0/g)^{1/2}$, where $\kappa_0$ is the thermal conductivity (assumed to be dominated by electron transport) and $D_e$ is the electron diffusion coefficient ($D_e = \kappa_0/C_e$). This results in a spatially distributed collection of acoustic sources, giving acoustic pulse broadening to a temporal duration $\sim z_e/v_l$ for $z_e > \zeta$). The relative values of $z_e$ and $\zeta$ therefore determine the importance of electron diffusion on the picosecond acoustic phonon generation. For liquid Hg, direct measurements of $\tau_e$ are not available, but we may estimate $g$ from the equation[47,48]

$$g = \frac{3\gamma\hbar\lambda\langle\omega^2\rangle}{\pi k_B}, \tag{4}$$

where $C_e = \gamma T_e$, $\lambda$ ($T_e$ the electron temperature) is the dimensionless electron-phonon coupling parameter, $\langle\omega^2\rangle$ is the mean-square phonon frequency, $\hbar$ is Planck's constant, and $k_B$ is Boltzmann's constant. Taking the value $\lambda \approx 1$ from solid Hg,[49] the known value of $\gamma (\approx 140\ \mathrm{J m^{-3}\ K^{-2}})$ for liquid Hg,[50] and assuming $\langle\omega^2\rangle \approx \omega_D^2$ for liquid Hg, where $\omega_D$ is the Debye frequency for Hg ($\approx 2\times 10^{13}$ rad $\mathrm{s^{-1}}$),[51] Eq. (4) gives $g \approx 400\times 10^{15}\ \mathrm{W m^{-3}\ K^{-1}}$. Using the known value of $\kappa_0$ ($\approx 7.8\ \mathrm{W m^{-1}\ K^{-1}}$)[44] gives $z_e \approx 5$ nm. Since $z_e \sim \zeta/2$, we conclude that electron diffusion will contribute a broadening effect to the acoustic pulses. As a rough estimate, instead of $\zeta$ one can substitute $\zeta + z_e \approx 3\zeta/2$ for an effective penetration depth. Incidentally, the above physical constants give $\tau_e \sim 0.1$ ps for $T_e \sim 300$ K. Our time resolution is not sufficient to test this estimate, a value not atypical for transition metals.[52] The relatively small value of $\tau_e$ implies that the broadening effect of electron diffusion takes place first before the onset of significant thermal diffusion.

We are now in a position to estimate the additional broadening effects of thermal diffusion. Provided that the thermal diffusivity $D (= \kappa_0/C)$ is reasonably small, the total broadening effect of thermal and electron diffusions is roughly determined by thermal diffusion during the acoustic propagation time $\tau_{ac} = (\zeta + z_e)/v_l$. The corresponding thermal diffusion length $z_i$ can be defined as $z_i = (D\tau_{ac})^{1/2}$. From the known values of $\kappa_0$ and $C (\approx 1.86\times 10^6\ \mathrm{J m^{-3}\ K^{-1}})$ for liquid Hg,[44] we find $z_i \approx 7$ nm, implying that the acoustic pulses are broadened by a factor $\lesssim (\zeta + z_e + z_i)/\zeta \sim 2$ by diffusion processes. The quantity $\zeta + z_e + z_i$ represents an upper limit for the effective penetration depth $\zeta'$. (Thermal diffusion from the Hg to the sapphire will also produce acoustic sources in the sapphire. However, we estimate that their strength is negligible compared to those in the Hg.)

The effect of the penetration $\zeta' \lesssim 2\zeta$ reduces the strain amplitude of the generated acoustic pulses by a factor of $\lesssim 2$. Our previous estimate of the initial strain amplitude should therefore be reduced to $\eta_0'/2 \sim 4\times 10^{-3}$ for the pump fluences used in experiment. This strain is still significantly larger than that, $\sim 10^{-4}$, normally encountered at similar fluences in solid metals. To check for nonlinear effects, we carried out a series of measurements at different pump fluences by varying the incident pump beam average power from the value (87 mW) used above down to ten times smaller, keeping the probe fluence constant. Both $\rho$ and $\delta\phi$ over the whole temporal range were found to vary strictly linearly with the pump power. Moreover, the shape of the echoes was unchanged. Given the pronounced strain pulse broadening on propagation, the peak strain amplitude of the acoustic pulse is quickly reduced from its initial value. For these reasons we shall therefore seek linear theories of acoustic propagation to explain our observed results.

Even accounting for the factor of $\lesssim 2$ that is expected to broaden the initially generated acoustic pulses compared to the predictions of the thermoelastic theory, there remains a large discrepancy between the observed acoustic echo duration ($\sim 100$ ps) and that predicted ($\sim 15$ ps). It is natural to consider acoustic dispersion processes to explain the pulse broadening observed in experiment. Before dealing with this problem we shall first turn to the theory of detection in order to clarify the relation between the results for $\rho$ and $\delta\phi$.

The presence of the strain $\eta(z,t)$ in the Hg and the displacement $u(t)$ of the Hg-sapphire interface leads to a change in the complex amplitude-reflection coefficient,[15,20,42,53]

$$\frac{\delta r(t)}{r} = \frac{4ikn_S\tilde{n}}{n_S^2 - \tilde{n}^2}\left(\frac{dn}{d\eta} + i\frac{d\kappa}{d\eta}\right)\int_0^\infty \eta(z',t)e^{2ik\tilde{n}z'}dz' + 2in_S k u(0,t), \tag{5}$$

where $n_S (=1.76)$[30] is the (ordinary) refractive index of the (transparent) sapphire, $\tilde{n} = n + i\kappa (= 2.6 + 5.9i)$ (Ref. 54) is the refractive index of liquid Hg, $dn/d\eta$ and $dk/d\eta$ are the photoelastic constants of liquid Hg, and $k$ is the optical vacuum wave number ($=2\pi/\lambda$, where $\lambda$ is the 750 nm probe wavelength). The integral in Eq. (5) arises from a sum of contributions to the photoelastic reflectance change from different depths in the sample within $\sim\zeta$. We do not include an extra term[42] due to the photoelastic effect in sapphire for reasons explained later. The second term in Eq. (5), equal in magnitude to $4\pi n_S u(z=0,t)/\lambda$, accounts for the extra optical path associated with the displacement $u$ (positive for the $+z$ direction that points into the Hg),

$$u(0,t) = -\int_0^\infty \eta(z',t)dz'. \tag{6}$$

Provided that the form of $\eta(z,t)$ is known, one can therefore predict the variation $\delta r(t)/r$.

For both the same-side and opposite-side experimental configurations, we must deal with a longitudinal-acoustic strain pulse that is reflected from the Hg-sapphire interface

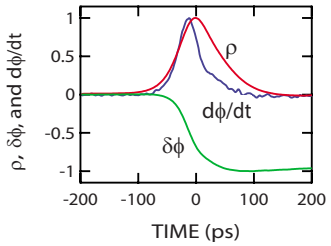


FIG. 4. (Color online) Normalized experimental variations in the optical amplitude-reflection coefficient $\rho$, the optical phase $\delta\phi$, and the time derivative $d\phi/dt$ for the first echo in a thin film of liquid Hg with a nominal thickness of 1.48 $\mu$m when pumping and probing from opposite sides of the sample. Zero time is defined at the peak of $\rho$.

with acoustic incidence from the Hg. When removed from the interface, let us assume that the strain pulse in the Hg has the temporal form $\eta_1(t)$, and spatiotemporal form

$$\eta(z,t) = \eta_1\left(t + \frac{z}{v_l}\right) + r_{ac}\eta_1\left(t - \frac{z}{v_l}\right). \tag{7}$$

We choose the time $t=0$ here to be the time for the strain pulse arrival at the interface (at $z=0$). Examination of Eq. (5), given the relatively long ($\sim$100 ps) strain pulse duration and corresponding spatial extent ($\sim$150 nm) in our experiment, suggests a considerable simplification of the analysis. The term $\exp(2i\tilde{n}kz') = \exp(-z'/\zeta)(2inkz')$ only has a significant value for $z' \lesssim \zeta(\approx 10$ nm). Assuming that the function $\eta_1(t)$ is slowly varying allows the integrals in Eq. (5) to be approximated, giving

$$\frac{\delta r(t)}{r} = \frac{2n_S}{\tilde{n}^2 - n_S^2}\left(\frac{dn}{d\eta} + i\frac{d\kappa}{d\eta}\right)\eta(0,t) + 2in_S ku(0,t). \tag{8}$$

The result is that $\rho(t) = \mathrm{Re}(\delta r/r) = \delta R(t)/(2R)$ is directly proportional to $\eta(0,t)$, the strain at the interface between the Hg and the sapphire. The phase $\delta\phi(t)$ is a linear combination of terms proportional to $\eta(0,t)$ and $u(0,t)$. The variation $\rho(t)$ is therefore a particularly useful quantity to monitor in the present experiment as it gives a direct measure of the strain pulse shape. This is thanks to the combination of the following circumstances: (1) the detection occurs at a buried interface at which the strain does not vanish, (2) the strain pulse spatial extent is much greater than the probe beam optical penetration depth in the Hg, and (3) the photoelastic response of the sapphire is negligible because the acoustic pulse (with a frequency of $\lesssim$10 GHz) contains negligible frequency components at the Brillouin frequency[40,55,56] $2n_S v_l'/\lambda(\sim 50$ GHz) of the sapphire [where $v_l' = 11100$ ms$^{-1}$ is the longitudinal sound velocity of sapphire perpendicular to a (0001) surface[29]].

In order to obtain a more accurate measure of the echo shape, higher-resolution data were taken in the region of $\pm$200 ps around the first echo for the opposite-side geometry, as shown in Fig. 4 for $\rho$ and $\delta\phi$ (plotted on the same scale) together with the variation $d\phi/dt$ (i.e., $d\delta\phi/dt$) for the first echo in a Hg film with a thickness of 1.48 $\mu$m. (The background variation in $\delta\phi$ is relatively small, and we have

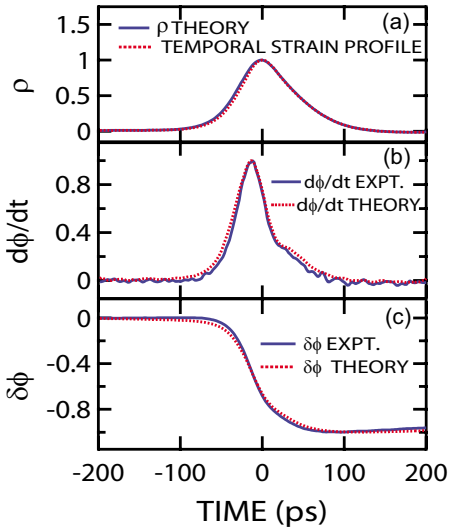


FIG. 5. (Color online) Comparison of the normalized theoretical predictions for the variations in optical amplitude-reflection coefficient $\rho$, optical phase $\delta\phi$, and time derivative $d\phi/dt$ according to a model in which the temporal strain profile is taken to be equal to the measured $\rho(t)$ for the first echo in a liquid Hg film with a nominal thickness of 1.48 $\mu$m using pumping and probing from the opposite side of the sample (as in Fig. 2). (a) Solid line: temporal strain profile. Dotted line: predicted variation $\rho(t)$ for this input strain profile. (b) Solid line: experimental $d\phi/dt$ variation. Dotted line: theoretical $d\phi/dt$ variation. (c) Solid line: experimental $\delta\phi$ variation. Dotted line: theoretical $\delta\phi$ variation.

not subtracted it from the data.) The quantity $d\phi/dt$ is also a useful quantity to plot because it is more directly related to the shape of the strain pulse compared to $\delta\phi$.[17] The asymmetry of $\rho(t)$ is particularly clear. Zero time is defined here to correspond to the maximum of $\rho(t)$. The shape of the $d\phi/dt$ variation is superficially similar to that of $\rho$, but $d\phi/dt$ is peaked slightly ($\sim$10 ps) before. The variation $\rho(t)$ allows us to immediately determine to a high accuracy the spatial shape of the strain pulse by use of the real part of Eq. (8): $\eta(z) \propto -\rho(-z/v_l)$, where the distance $z$ (=0 at the center of the strain pulse) is defined as the direction to the right in the inset of Fig. 2. The negative sign multiplying $\rho$ is chosen because a compressive strain pulse is expected. (This is experimentally justified by the sign of $\delta\phi$.) The strain pulse $\eta(z)$, determined in this way using the known value of $v_l$, is plotted as the dashed line in Fig. 3. Clearly the strain pulse is significantly broadened compared to the initial strain profile calculated according to the thermoelastic model (as shown by the solid line in Fig. 3).

Measuring both $\delta\phi(t)$ and $\rho(t)$ allows the photoelastic constants $dn/d\eta$ and $dk/d\eta$ to be derived. We proceed by assuming a negative incident strain in the form of the experimental variation $\rho(t)$ (as in the dashed line in Fig. 3) and then use Eqs. (5)–(7) to obtain the resulting $\rho$, $\delta\phi$, and $d\phi/dt$ variations. The method of least squares is used to fit these variations to the data using only the photoelastic constants $dn/d\eta$ and $d\kappa/d\eta$ as adjustable parameters. The best fits are shown in Fig. 5 by the dotted lines using $(dn/d\eta)/(d\kappa/d\eta) = -0.85(\pm 0.1)$ and $dn/d\eta = 17(\pm 7)$ (at our 750 nm optical wavelength), where the errors reflect the scat-

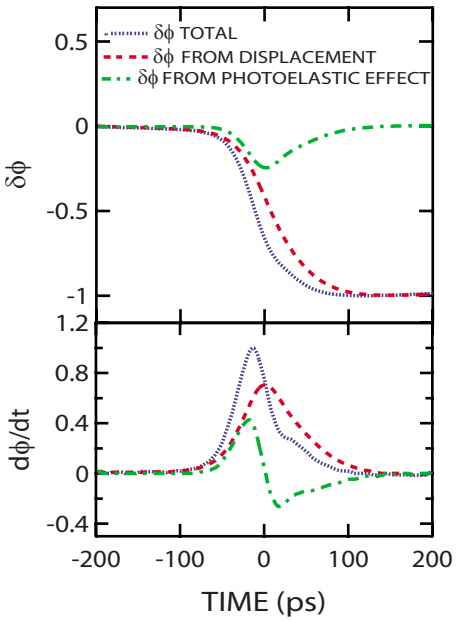


FIG. 6. (Color online) Plots of the normalized variations in optical phase $\delta\phi$ and time derivative $d\phi/dt$ (dotted lines) according to the theoretical model, showing in addition the components of the variations arising from the photoelastic effect (dashed-dotted lines) and the surface displacement (dashed lines).

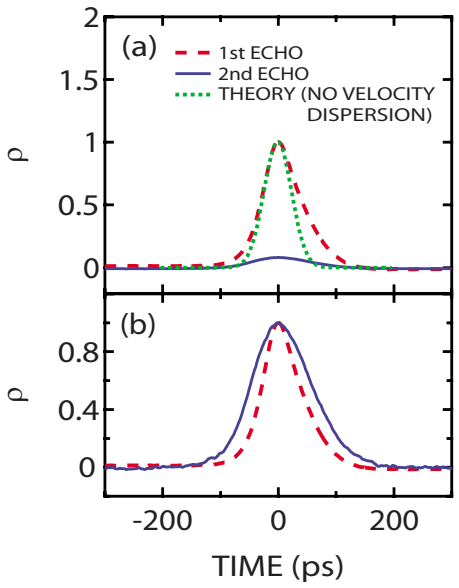


FIG. 7. (Color online) (a) Comparison between the normalized variation in the optical amplitude-reflection coefficient $\rho$ for the first echo (dashed curve) and the second echo (solid curve) in a thin film of liquid Hg with a nominal thickness of 1.48 $\mu$m when pumping and probing from opposite sides of the sample. The dotted curve shows the theoretical prediction when only frequency-dependent ultrasonic attenuation is incorporated in the model using the thermoelastic theory of the generation process. (b) The same two experimental variations for $\rho$ as in (a) except that the data for the second echo is also normalized to 1 (for ease of observation of the difference in temporal profiles). The time between the two echoes is 2022 ps.

ter of different measurements.[57] We are not aware of any literature values for comparison. As expected, the derived variation $\rho(t)$ is essentially the same as the assumed strain pulse shape shown by the solid line in Fig. 5(a) (tiny differences only arising because of the slight smoothing caused by the probe beam penetration into the Hg). This confirms the validity of the approximation of Eq. (8). The derived variations for $d\phi/dt$ and $\delta\phi$, shown by the dotted lines in Figs. 5(b) and 5(c), respectively, are also in good agreement with experiment (solid lines); in particular, the peak in $d\phi/dt$ occurs slightly before that of $\rho(t)$, as required. The shape of the derived $\delta\phi$ and $d\phi/dt$ variations is sensitive to the ratio $dn/d\eta$:$d\kappa/d\eta$ and to the sign of these constants, whereas the ratio of the variations $\rho(t)$ and $\delta\phi(t)$ depends on the absolute values of the photoelastic constants.[57]

Unlike $\rho(t)$, which arises purely from the photoelastic effect, the $\delta\phi$ and $d\phi/dt$ variations are made up of contributions from both the photoelastic effect and surface displacements. These contributions to $\delta\phi$ and $d\phi/dt$ are shown in Fig. 6. The displacement contribution to $d\phi/dt$, shown by the dashed line in the lower plot, is the same as the strain pulse shape [as expected from Eqs. (6) and (7)]. The contributions from the photoelastic effect, shown by the dashed-dotted lines in Fig. 6, are significant in both $\delta\phi$ and $d\phi/dt$, and the photoelastic contribution is responsible for the slight temporal advance in the peak of $d\phi/dt$.

## IV. RESULTS FOR THE ACOUSTIC DISPERSION

Let us now turn to the analysis of the echo shape, focusing on the variation $\rho(t)$. Figure 7(a) shows on the same scale the first and second echoes (dashed and solid lines) for $\rho$ obtained with opposite-side detection for the 1.48 $\mu$m film of Hg of Fig. 4. The height of the two echoes is adjusted to be the same for better comparison in Fig. 7(b), demonstrating the broadening effect of propagation. Background-subtracted results obtained with same-side detection for a 1.47 $\mu$m film of Hg are shown in Fig. 8. (The relative noise level for the second echo is noticeably larger owing to the longer propagation distance.)

The measurement of two echoes allows the extraction of the dispersion in the ultrasonic attenuation. This has previously been reported in picosecond laser acoustics for a variety of thin films.[15,32,58,59] As is common in lower frequency acoustic pulse-echo measurements,[60,61] the dispersion in the sound velocity may also be extracted. To this end we decompose the initial acoustic wave packet (when free from the near-surface region) in the form

$$f(z,t) = \int_{-\infty}^{\infty} F(z,\omega)e^{-i\omega t}d\omega, \tag{9}$$

$$F(z,\omega) = \frac{1}{2\pi}\int_{-\infty}^{\infty} f(z,t)e^{-i\omega t}dt, \tag{10}$$

and assume only propagation in the $+z$ direction (since the effect of acoustic reflections from the Hg-sapphire interface can be accounted for by multiplying the acoustic strain pulse

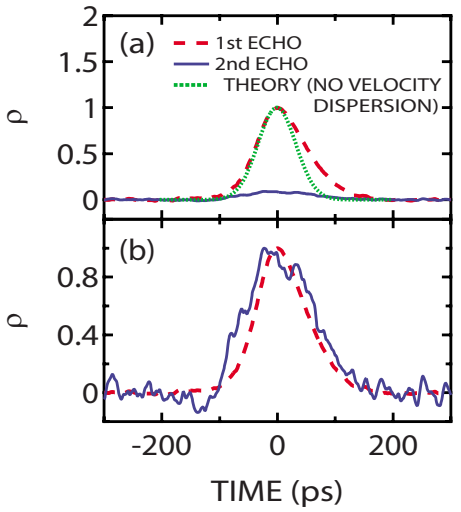


FIG. 8. (Color online) (a) Comparison between the normalized variation in the optical amplitude-reflection coefficient $\rho$ for the first echo (dashed curve) and the second echo (solid curve) in a thin film of liquid Hg with a nominal thickness of 1.47 $\mu$m when pumping and probing from the *same* side of the sample. The dotted curve shows the theoretical prediction when only frequency-dependent ultrasonic attenuation is incorporated in the model using the thermoelastic theory of the generation process. (b) The same two experimental variations for $\rho$ as in (a) except that the data for the second echo is also normalized to 1 (for ease of observation of the difference in temporal profiles). The time between the two echoes is 2026 ps.

by a constant). We may then expand the real function $f(z,t)$ in the general form

$$f(z,t) = \frac{1}{2}\int_0^\infty F_0(\omega)e^{ik(\omega)z}e^{-i\omega t}d\omega + \frac{1}{2}\int_{-\infty}^0 F_0^*(-\omega)e^{-ik^*(-\omega)z}e^{-i\omega t}d\omega,$$

where $\tilde{k}=k_1+ik_2$ is the complex acoustic wave number, $F_0(\omega)$ is a function defined for $\omega>0$ that represents the acoustic spectrum, and $^*$ represents the complex conjugate. If the same time origin is chosen for two consecutive echoes, and $t=0$ is defined at the first echo, then

$$F(0,\omega) = \frac{1}{2}F_0(\omega),$$

$$F(z',\omega) = \frac{1}{2}r_{ac}^2F_0(\omega)e^{ik_1(\omega)z'}e^{-k_2(\omega)z'},$$

where $z'$ is now defined as the propagation distance and $r_{ac}$ is the acoustic reflection coefficient from the Hg-sapphire interface (assumed to be independent of $\omega$ to a good approximation[62]). It is convenient to define the origin of time for the second echo in its vicinity ($t=t'$). In that case $F(z',\omega)$ should be replaced by

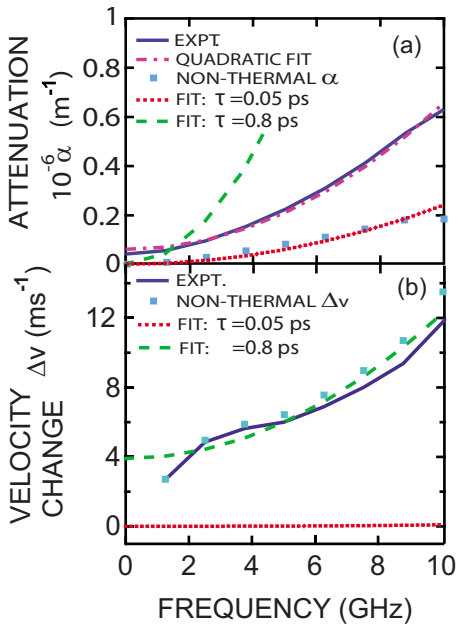


FIG. 9. (Color online) (a) Ultrasonic attenuation coefficient $\alpha$ and (b) phase velocity change $\Delta v$ plotted as a function of frequency for a thin film of liquid Hg with a nominal thickness of 1.48 $\mu$m when pumping and probing from opposite sides of the sample. Solid curves: experimentally derived variations. Dashed-dotted curve: least-squares fit to $\alpha$ with a quadratic frequency variation. Solid squares: experimental contribution to $\alpha$ and $\Delta v$ from structural relaxation (with the constant contribution to $\alpha$ and the calculated thermal contributions to $\alpha$ and $\Delta v$ subtracted out). Dashed curves: theoretical predictions from the simple structural relaxation model with single time constant $\tau=0.8$ ps. Dotted curves: the same with time constant $\tau=0.05$ ps. (The absolute position of the dashed curve for $\Delta v$ has been offset to fit the data.)

$$G(z',\omega) = \frac{1}{2}r_{ac}^2F_0(\omega)e^{ik_1(\omega)z'}e^{-k_2(\omega)z'}e^{-i\omega t'}, \quad (11)$$

as can be seen by replacing $f(z,t)$ by $f(z,t+t')$ in Eq. (10). It is now straightforward to derive the dispersions $k_1(\omega)$ and $k_2(\omega)$ from the real part and modulus of the following equation:

$$\frac{G(z',\omega)}{F(0,\omega)} = r_{ac}^2e^{i[k_1(\omega)z'-\omega t']}e^{-k_2(\omega)z'},$$

where $k_1(\omega)=\omega/v(\omega)$ is related to phase velocity $v(\omega)$ (where $v=v_l$) and $k_2(\omega)=\alpha(\omega)$ is the ultrasonic amplitude attenuation coefficient. When applying this method, one must ensure that the phase $k_1(\omega)z'-\omega t'$ over the frequency spectrum of the pulse should be known without ambiguity. For the Hg film thicknesses in question this is not a problem because the phase variation remains within $\pi/2$.[63] This analysis also requires a knowledge of the film thickness, derived in this study using the low-frequency longitudinal sound velocity of liquid Hg. In this respect our measurements of the velocity dispersion are accurate for the relative changes as a function of frequency, but do not provide an absolute determination of $v_l$.[64]

The solid curve in Fig. 9(a) shows the measured disper-

sions using the opposite-side results of Figs. 4–7. The attenuation can be fitted by the equation $\alpha(f)=A+Bf^2$ (dashed-dotted line) with $B=6000\ \mathrm{m^{-1}\ GHz^{-2}}$, a value in reasonable agreement with $B=5700\ \mathrm{m^{-1}\ GHz^{-2}}$ determined at frequencies below 1 GHz at room temperature.[3] The nonzero value found for $A=85\,000\ \mathrm{m^{-1}}$, not expected in liquid metals, is likely to be an artifact of the choice of the acoustic reflection coefficient ($r_{ac}=0.39$) assumed for the Hg-sapphire boundary. The value of $A$ only affects the echo height, not the echo shape. The reflection coefficient $r_{ac}$ may be lower than the calculated value (reducing the value of $A$) if the sound velocity is slightly higher than the low-frequency value $v_l=1450\ \mathrm{ms^{-1}}$ assumed. Another possible cause might be the presence of imperfect interfaces.[65] At room temperature it is known that liquid Hg does not wet sapphire, precluding the possibility of interdiffusion.[66,67] However, the surface roughness of the sapphire, measured to be $\sigma\sim 3$ nm rms, can introduce a frequency-dependent ultrasonic reflection coefficient $r'_{ac}(\omega)$, where $r'^2_{ac}(\omega)=r^2_{ac}\exp(-\omega^2\sigma^2/v_l^2)$,[68,69] since account should be taken of two reflections (relevant to the comparison of the first and second echoes). In comparison with the magnitude of $\alpha(f)$ and propagation distances in question here for Hg, the effect of this surface roughness is not significant. [Owing to the experimental uncertainty in measuring $\alpha(f)$, we have not attempted to correct $\alpha(f)$ for the slight effect of surface roughness.] Yet another possible cause is slight changes in the optical spot size at the sample surface as a function of the optical delay (associated with the use of Gaussian optical beams). Since it is the constant $B$ that is of most interest, we did not pursue this point further. Measurements on other Hg films with thicknesses of $\sim 1\ \mu$m give $B=6000\pm 2000\ \mathrm{m^{-1}\ GHz^{-2}}$. A more general fit to $\alpha(f)$ in the form of a power law is also possible, as discussed in Sec. V.

The constant $B$ determines the distortion of the strain pulse caused by ultrasonic attenuation. It is interesting to calculate the expected form of the strain pulses when including only this effect in the case when the $Bf^2$ variation of $\alpha$ holds up to the frequencies, $\lesssim 100$ GHz, contained in the initial acoustic pulse. Starting with the thermoelastic model for the initial strain profile shown in Fig. 3, we have calculated the strain pulse shape at the time of the first echo in Figs. 7(a) and 8(a) for the opposite-side and same-side results, respectively (see dotted lines). Although in both cases the leading edges of the echoes are reproduced well, the predicted strain pulse shapes fail to account for the asymmetric broadening of the trailing edges. This result is not affected by the broadening of the initial strain pulse through diffusion processes because the high-frequency components of the acoustic pulse are removed by the frequency-dependent attenuation. These considerations show that the dispersion in the sound velocity is essential to understand the observed echo shapes.

In the absence of a well-known functional form for the sound velocity variation $\Delta v(f)$, we shall not attempt to reproduce the first echo shape including velocity dispersion. Instead we use Eq. (11) to calculate the velocity dispersion. The result is shown by the solid curve in Fig. 9(b). [The absolute value of $\Delta v$ is adjusted to make $\Delta v(f\to 0)\approx 0$.] Over the accessible acoustic frequency range (1–10 GHz), the sound velocity increases approximately linearly. A positive dispersion, approximately linearly increasing with frequency, was also recorded for other Hg film thicknesses of $\sim 1\ \mu$m.[70] This velocity dispersion has not been detected in liquid Hg at lower frequencies ($<1$ GHz).[71,72] Interpretation in terms of a more general $\Delta v(f)$ variation in the form of a power law in frequency is also possible, as discussed in Sec. V.

## V. DISCUSSION AND CONCLUSIONS

The simplest approach to understand these results for dispersion is to make use of the standard models for structural[2] and thermoelastic relaxation in liquids. At low frequencies (well below the reciprocals of the volume and shear relaxation times $1/\tau_v$ and $1/\tau_s$, respectively), under approximately adiabatic conditions, and for $\alpha v/\omega \ll 1$ (as for our case), the following equations apply:

$$\alpha=\frac{1}{2v}\left[\frac{B_\infty-B_0}{B_0}\tau_v+\frac{4}{3}\frac{G_\infty}{B_0}\tau_s+\frac{(\gamma-1)D}{v^2}\right]\omega^2, \qquad (12)$$

$$\frac{\Delta v}{v}=\frac{1}{2}\left[\frac{B_\infty-B_0}{B_0}\tau_v^2+\frac{4}{3}\frac{G_\infty}{B_0}\tau_s^2-\frac{(\gamma-1)D^2}{2v^4}\right]\omega^2, \qquad (13)$$

where $B_0$ and $B_\infty$ are, respectively, the low- and infinite-frequency bulk moduli, $G_\infty$ is the infinite-frequency shear modulus, $v$ is a shorthand for the adiabatic longitudinal velocity, $\gamma$ is the ratio of the specific heats ($\gamma=c_P/c_V=1.15$),[73] and $D$ is the thermal diffusivity. The terms proportional to $\gamma$-1 result from the thermal diffusion associated with stress-induced temperature changes and are correct under approximately adiabatic conditions that hold provided that frequencies are *small* compared to $v^2/(2\pi\gamma D)\approx 70$ GHz.[74] One can see that associated with the characteristic $\omega^2$ dependence of the ultrasonic attenuation coefficient is a velocity dispersion that also varies with $\omega^2$. (In the absence of structural relaxation, the longitudinal sound velocity falls from its adiabatic value $v$ to its isothermal value $v/\sqrt{\gamma}$ as the frequency is increased.) We estimate that the thermal term in $\alpha$ amounts to a contribution of $4100\ \mathrm{m^{-1}\ GHz^{-2}}$ to the coefficient $B$.[73] In addition, by writing $\Delta v=B'\omega^2$ we estimate that the thermal term in the sound velocity change $\Delta v$ amounts to a contribution of $-0.017\ \mathrm{ms^{-1}\ GHz^{-2}}$ to the coefficient $B'$. Subtracting these quantities from our experimental data for $\alpha$ and $\Delta v$ allows the evaluation of the "nonthermal" contribution to these quantities, as shown by the square symbols in Fig. 9 (ignoring the constant term $A$ in $\alpha$). These are the parts of the attenuation and velocity dispersion that are expected to arise from structural relaxation.

For a quantitative theory one needs to make assumptions concerning the relaxation times. If we assume for simplicity an identical value $\tau$ for the volume and shear relaxation times, Eqs. (12) and (13) provide a well-defined relation between the variations $\alpha(\omega)$ and $\Delta v(\omega)$. Figure 9 shows the predicted variations of the nonthermal components of the velocity dispersion and attenuation under the following assumptions: $(B_\infty-B_0)/B_0=1$ (in rough accord with the large dispersion in the sound velocity[13]), $G_\infty/B_0=1.7$ (in accord

with the ratio of the measured bulk to shear viscosities in liquid Hg[3]), with $\tau=0.05$ ps (dotted lines) and 0.8 ps (dashed lines). For $\tau=0.05$ ps the frequency dependence of the nonthermal component of $\alpha$ is approximately reproduced but the nonthermal component of $\Delta v$ is underestimated, whereas in the latter case the frequency dependence of the nonthermal component of $\Delta v$ is approximately reproduced but the nonthermal component of $\alpha$ is overestimated. In addition, the predicted quadratic variation in $\Delta v$ does not agree with the approximately linear rise observed in experiment. When $\tau=0.8$ ps this simple model gives the same order of magnitude for $\tau$ as that obtained from neutron-scattering studies ($\tau\sim 1$ ps).[75]

It is possible to obtain a better fit to both the velocity dispersion and attenuation if the parameters $(B_\infty-B_0)/B_0$ and $G_\infty/B_0$ are varied and if we abandon the low-frequency approximation for the structural relaxation to allow for lower values of $\tau_s$ and $\tau_v$.[2] For example, we could obtain reasonably good fits to our data in this way using $(B_\infty-B_0)/B_0=0.005$, $G_\infty/(B_\infty-B_0)=1.7$ (as above), and $\tau=15$ ps, giving approximately quadratic and linear dependences of $\alpha$ and $\Delta v$ with $\omega$, respectively. This result with $(B_\infty-B_0)/B_0\ll 1$, however, does not agree with the expected significant high-frequency stiffening observed in liquid Hg in other experiments.[13] There are in fact a wide range of possible models including those with a distribution of relaxation times.[2,76] For example, our results can be reproduced by combining a relaxation time $\tau_1=15$ ps associated with the reduced values of $(B_\infty-B_0)/B_0$ and $G_\infty/B_0$ above with a relaxation time $\tau_2\lesssim 0.01$ ps associated with the values $(B_\infty-B_0)/B_0=1$ and $G_\infty/B_0=1.7$. However, given the limited frequency range of our measurements we cannot distinguish between these different possibilities.

Further insight into these results for dispersion can be obtained by applying the relevant Kramers-Krönig relations arising from the requirements of causality in acoustics:[77–79] it has been shown that in the case when the experimental attenuation can be approximated as a power law, it is particularly straightforward to predict the velocity change from the measured attenuation.[79,80] In Fig. 10(a) we have fitted the frequency-dependent component of the measured ultrasonic attenuation to the law $\alpha(\omega)=\alpha_0\omega^y$, where $y=1.7$ for the best fit in the frequency range up to 10 GHz (with $\alpha_0=2.6\times 10^{-13}$ when $\omega$ is expressed in rad $s^{-1}$). (The relatively small deviation of the optimum value of $y=1.7$ from the value $y=2$ explains why we were previously also able to fit with the latter value.) This fit with $y=1.7$ is shown by the dotted curve in Fig. 10(a), and agrees extremely well with the data (solid curve). The Kramers-Krönig relations for $1<y<3$ yield $\Delta v=-\alpha_0 v^2\omega^{y-1}\tan[y\pi/2]$ when $\omega=0$ is taken as a reference frequency.[79,80] For the case $y=1.7$ one therefore obtains $\Delta v\approx 0.51\alpha_0 v^2\omega^{0.7}$. The predicted $\Delta v(\omega)$ based on the fit in Fig. 10(a) is shown by the dotted line in Fig. 10(b). The agreement with experiment is good, suggesting that the power-law variation of $\alpha(\omega)$ extends beyond the frequency range probed. These power-law variations that we obtain for $\alpha(\omega)$ and $\Delta v(\omega)$ emphasize that valid theories for the experimental behavior probably do not involve a single relaxation time.

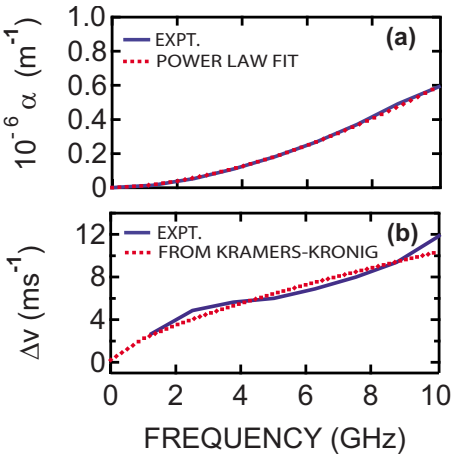


FIG. 10. (Color online) (a) Ultrasonic attenuation coefficient $\alpha$ and (b) phase velocity change $\Delta v$ plotted as a function of frequency for a thin film of liquid Hg with a nominal thickness of 1.48 $\mu$m when pumping and probing from opposite sides of the sample. Solid curves: experimentally derived variations. A constant attenuation has been subtracted from the experimental $\alpha$. Dotted curve in (a): fit to the frequency dependent component of $\alpha$ with a power-law variation: $\alpha\propto f^{1.7}$. Dotted curve in (b): prediction for $\Delta v$ from the Kramers-Krönig relations. (The vertical position of the experimental curve for $\Delta v$ is chosen for a good fit.)

In conclusion, we have investigated the generation of sound in a liquid metal with ultrashort light pulses. We excite and interferometrically detect picosecond longitudinal-acoustic pulses in thin films of a liquid mercury sandwiched between sapphire plates. By analyzing consecutive echoes we derive the dispersion in the ultrasonic attenuation and in the sound velocity for this liquid at frequencies up to 10 GHz. The observed structural relaxation produces strong broadening and asymmetric distortion of the acoustic pulses. The magnitude of both the velocity dispersion and ultrasonic attenuation dispersion suggest the presence of picosecond relaxation times in liquid mercury.

In addition, we have shown how the longitudinal strain pulse shape in mercury can be directly probed using detection at a buried interface. This allowed us to measure the characteristic asymmetric strain pulse shape caused by acoustic velocity dispersion. This strain detection method should prove useful for analyzing the ultrafast optical generation and propagation of strain in opaque liquids under conditions in which the probe optical penetration depth is small compared to the spatial extent of the acoustic pulses. Measurements on thinner liquid films, perhaps down to below 100 nm in thickness, should allow the investigation of structural or thermoelastic relaxation at frequencies up to 100 GHz. This method should apply equally well to other liquid metals or to opaque liquids in general.

[1] K. F. Herzfeld and T. A. Litovitz, *Absorption and Dispersion of Ultrasonic Waves* (Academic, London, 1968).
[2] T. A. Litovitz and C. M. Davis, in *Physical Acoustics*, edited by W. P. Mason (Academic, New York, 1965), Vol. 2A, p. 281.
[3] G. M. B. Webber and R. W. B. Stephens, in *Physical Acoustics*, edited by W. P. Mason (Academic, New York, 1968), Vol. 4B, p. 53.
[4] U. Kaatze, T. O. Hushcha, and F. Eggers, J. Solution Chem. **29**, 299 (2000).
[5] J.-P. Monchalin and J.-D. Aussel, J. Nondestruct. Eval. **9**, 211 (1990).
[6] B. F. Pouet and N. J. P. Rasolofosaon, J. Acoust. Soc. Am. **93**, 1286 (1993).
[7] R. D. Mountain, Rev. Mod. Phys. **38**, 205 (1966).
[8] C. J. Montrose, V. A. Solovyev, and T. A. Litovitz, J. Acoust. Soc. Am. **43**, 117 (1968).
[9] G. I. A. Stegeman and B. P. Stoicheff, Phys. Rev. A **7**, 1160 (1973).
[10] E. W. Fischer, Physica A **201**, 183 (1993).
[11] F. Sette, M. H. Krisch, C. Masciovecchio, G. Ruocco, and G. Monaco, Science **280**, 1550 (1998).
[12] E. Burkel, Rep. Prog. Phys. **63**, 171 (2000).
[13] T. Scopigno and G. Ruocco, Rev. Mod. Phys. **77**, 881 (2005).
[14] B. Frick, C. Alba-Simionesco, G. Dosseh, C. L. Quellec, A. J. Moreno, J. Colmenero, A. Schönhals, R. Zorn, K. Chrissoupoulou, S. H. Anastasiadis, and K. Dalnoki-Veress, J. Non-Cryst. Solids **351**, 2657 (2005).
[15] C. Thomsen, H. T. Grahn, H. J. Maris, and J. Tauc, Phys. Rev. B **34**, 4129 (1986).
[16] H. T. Grahn and J. Tauc, IEEE J. Quantum Electron. **25**, 2562 (1989).
[17] O. B. Wright and K. Kawashima, Phys. Rev. Lett. **69**, 1668 (1992).
[18] V. E. Gusev and A. A. Karabutov, *Laser Optoacoustics* (American Institute of Physics, Woodbury, NY, 1993).
[19] O. Matsuda, T. Tachizaki, T. Fukui, J. J. Baumberg, and O. B. Wright, Phys. Rev. B **71**, 115330 (2005).
[20] B. Perrin, *Microscale and Nanoscale Heat Transfer*, Topics in Applied Physics Vol. 107 (Springer-Verlag, Berlin, 2007), p. 333.
[21] S. Ruhman, A. G. Joly, and K. A. Nelson, IEEE J. Quantum Electron. **24**, 470 (1988).
[22] L. J. Shelton, F. Yang, W. K. Ford, and H. J. Maris, Phys. Status Solidi B **242**, 1379 (2005).
[23] G. Tas and H. J. Maris, Phys. Rev. B **55**, 1852 (1997).
[24] M. W. Sigrist, J. Appl. Phys. **60**, R83 (1986).
[25] B.-M. Kim, A. M. Komashko, A. M. Rubenchik, M. D. Feit, S. Reidt, and L. B. Da Silva, J. Appl. Phys. **94**, 709 (2003).
[26] J. G. Dil and E. M. Brody, Phys. Rev. B **14**, 5218 (1976).
[27] O. B. Wright, Phys. Rev. B **49**, 9985 (1994).
[28] Samples of 99.999% purity were used as well as samples of unknown purity. Similar echo shapes were observed for all samples.
[29] O. L. Anderson, in *Physical Acoustics*, edited by W. P. Mason (Academic, New York, 1965), Vol. 3B, p. 43.
[30] *Electronic Handbook of Optical Constants of Solids*, edited by E. D. Palik and G. Ghosh (Academic, San Diego, 1999).
[31] G. Tas and H. J. Maris, Phys. Rev. B **49**, 15046 (1994).
[32] T. Saito, O. Matsuda, and O. B. Wright, Phys. Rev. B **67**, 205421 (2003).
[33] The maximum transient temperature rise can be estimated using the expression $Q(1-R)/AC\zeta'$, where $Q$ is the energy of a single incident optical pump pulse, $R \approx 0.7$ is the optical reflectance of the pump beam from the sample (including the front face of the sapphire), $A=\pi w^2/2$ is the pump beam-spot area, $C$ is the specific heat per unit volume of liquid Hg, and $\zeta'$ is the effective penetration depth of the pump beam into the Hg, taken to be $\sim$20 nm (as explained in Sec. III). The spot radius $w=17.5$ $\mu$m is obtained from the pump beam lateral intensity profile, given by $I(r)=\exp(-2r^2/w^2)$. There is a simple relation between $w$ and the full intensity width at half maximum $D$ in this case: $w \approx 0.85D$. In our case $Q(1-R)$ is equal to 0.7 nJ. The steady-state temperature rise of the sample at the center of the optical pump spot can be estimated from the expression $P(1-R)/(2\pi)^{1/2}w\kappa_S$, where $P$ is the average power of the (chopped) optical pump beam and $\kappa_S$ is the thermal conductivity of the sapphire substrate. The presence of the Hg has a negligible effect on this steady-state temperature rise. In our case $P(1-R)$ is equal to 27 mW; The value of $\kappa_S$ was taken from, *Thermal Conductivity: Nonmetallic Solids*, Thermophysical Properties of Matter Vol. 2, edited by Y. S. Touloukian, R. W. Powell, C. Y. Ho, and P. G. Klemens (Plenum, New York, 1970); The value of $C$ was taken from the *American Institute of Physics Handbook*, 3rd ed., edited by D. E. Gray (McGraw-Hill, New York, 1972); The refractive index of sapphire and liquid Hg at 750 nm were taken to be equal to 1.76 and $2.6+5.9i$, obtained from the *Electronic Handbook of Optical Constants of Solids* (Ref. 30).
[34] J. B. Walter, K. L. Telschow, and R. J. Conant, in *Review of Progress in Quantitative Nondestructive Evaluation*, edited by D. O. Thomsen and D. E. Chimenti (Plenum, New York, 1995), Vol. 14, p. 507.
[35] E. Fraizier, M.-H. Nadal, and R. Oltra, J. Appl. Phys. **93**, 649 (2003).
[36] H. Nakano, Y. Matsuda, and S. Nagai, Meas. Sci. Technol. **9**, 617 (1998).
[37] B. Perrin, B. Bonello, J.-C. Jeannet, and E. Romatet, Prog. Nat. Sci. **S6**, 444 (1996).
[38] D. H. Hurley and O. B. Wright, Opt. Lett. **24**, 1305 (1999).
[39] O. B. Wright, B. Perrin, O. Matsuda, and V. E. Gusev, Phys. Rev. B **64**, 081202 (2001).
[40] O. B. Wright, J. Appl. Phys. **71**, 1617 (1992).
[41] O. B. Wright, Opt. Lett. **20**, 632 (1995).
[42] O. Matsuda and O. B. Wright, J. Opt. Soc. Am. B **19**, 3028 (2002).
[43] For a spatially Gaussian pump spot with $1/e^2$ intensity radius $w$, $A=\pi w^2/2$ when $Q/A$ corresponds to the energy density at the centre of the spot.
[44] *American Institute of Physics Handbook*, 3rd ed., edited by D. E. Gray (McGraw-Hill, New York, 1972).
[45] O. B. Wright and V. E. Gusev, IEEE Trans. Ultrason. Ferroelectr. Freq. Control **42**, 331 (1995).
[46] V. E. Gusev and O. B. Wright, Phys. Rev. B **57**, 2878 (1998).
[47] P. B. Allen, Phys. Rev. B **3**, 305 (1971).
[48] P. B. Allen, Phys. Rev. Lett. **59**, 1460 (1987).
[49] W. L. McMillan, Phys. Rev. **167**, 331 (1968).
[50] N. W. Ashcroft and N. D. Mermin, *Solid State Physics* (Holt-Saunders, Orlando, 1976).
[51] C. Kittel, *Solid State Physics*, 8th ed. (Wiley, New York, 2005).
[52] S. D. Brorson, A. Kazeroonian, J. S. Moodera, D. W. Face, T. K.

Cheng, E. P. Ippen, M. S. Dresselhaus, and G. Dresselhaus, Phys. Rev. Lett. **64**, 2172 (1990).
[53] V. E. Gusev, Acust. Acta Acust. **82**, S37 (1996).
[54] *CRC Handbook of Chemistry and Physics*, edited by D. R. Lide (CRC, Boca Raton, FL, 2004).
[55] For the transparent sapphire, the exponential term in the integral of Eq. (5) ensures that only acoustic waves at frequency $2n_s v_1'/\lambda$ are detected.
[56] H. N. Lin, R. J. Stoner, H. J. Maris, and J. Tauc, J. Appl. Phys. **69**, 3816 (1991).
[57] The ratio of the height of the $\rho$ echo to the step of the $\delta\phi$ echo was observed to be 1.4 for the data of Figs. 4 and 5. Some variation in this ratio was observed over different measurements, so the absolute values of $dn/d\eta$ and $dk/d\eta$ are subject to a $\sim$40% error.
[58] T. C. Zhu, H. J. Maris, and J. Tauc, Phys. Rev. B **44**, 4281 (1991).
[59] J.-Y. Duquesne and B. Perrin, Phys. Rev. B **68**, 134205 (2003).
[60] W. Sachse and Y.-H. Pao, J. Appl. Phys. **49**, 4320 (1978).
[61] D. Schneider, T. Schwarz, and B. Schultrich, Thin Solid Films **219**, 92 (1992).
[62] We have estimated the effect of the frequency-dependent sound velocity and ultrasonic attenuation on the acoustic reflection coefficient $r_{ac}(\omega)$ using the simple models of relaxational processes described in Sec. V. We find that the contribution to the apparent velocity dispersion and ultrasonic attenuation in the measured data from this source in our case is negligible.
[63] The accuracy of the analysis for the determination of the dispersion in velocity and attenuation was checked using synthesized acoustic pulses with dispersion and attenuation similar to that of Hg. The numerical error in this process is negligible compared to the scatter in the data for different Hg films.
[64] Strictly speaking, an independent measurement of $z'$ is required to determine the dispersion. However, if the velocity dispersion is small, as is expected to be the case for liquid Hg below 10 GHz, it is a good approximation to estimate $z'$ from the time between the maxima of the first and second echoes and from the known low-frequency sound velocity.
[65] C. J. K. Richardson, M. J. Ehrlich, and J. W. Wagner, J. Acoust. Soc. Am. **107**, 1987 (2000).
[66] Y. Ohmasa, Y. Kajihara, H. Kohno, Y. Hiejima, and M. Yao, J. Non-Cryst. Solids **250-252**, 209 (1999).
[67] J. Vollmann, D. M. Profunser, and J. Dual, Rev. Sci. Instrum. **74**, 851 (2003).
[68] This estimate is based on a Gaussian distribution of surface heights for the two sapphire surfaces.
[69] S. A. Akhmanov and V. E. Gusev, Sov. Phys. Usp. **35**, 153 (1992).
[70] The gradient of the positive dispersion $dv/d\omega$ is known to an accuracy $\sim$50%.
[71] G. R. Ringo, J. W. Fitzgerald, and B. G. Hurdle, Phys. Rev. **72**, 87 (1947).
[72] J. Jarzynski, Proc. Phys. Soc. London **81**, 745 (1963).
[73] The thermal contribution can be simply estimated with the help of the relation $\gamma-1=T\beta^2B/C_V=T\beta^2\rho_0 v_l^2/C_V$.
[74] This can be seen by Taylor expansion of the solution of a biquadratic equation proposed by Thurston: R. N. Thurston, in *Physical Acoustics*, edited by W. P. Mason (Academic, New York, 1964), Vol. 1A, p. 1. See Eq. (258).
[75] L. E. Bove, F. Sacchetti, C. Petrillo, B. Dorner, F. Formisano, M. Sampoli, and F. Barocchi, J. Non-Cryst. Solids **307-310**, 842 (2002).
[76] W. H. Nichols and E. F. Carome, J. Chem. Phys. **49**, 1000 (1968).
[77] H. M. Nussenzveig, *Causality and Dispersion Relations* (Academic, New York, 1972).
[78] R. L. Weaver and Y.-H. Pao, J. Math. Phys. **22**, 1909 (1981).
[79] T. L. Szabo, J. Acoust. Soc. Am. **97**, 14 (1995).
[80] K. R. Waters, M. S. Hughes, J. Mobley, G. H. Brandenburger, and J. G. Miller, J. Acoust. Soc. Am. **108**, 556 (2000).